Research Article | Vol. 9, No. 10 / 1 October 2019 / Optical Materials Express 4009
Optical Materials EXPRESS

One-dimensional photonic crystal for Bloch surface waves and radiation modes-based sensing

M. Gryga,[1] D. Vala,[2] P. Kolejak,[2] L. Gembalova,[1] D. Ciprian,[1] and P. Hlubina[1,*]

[1]Department of Physics, Technical University Ostrava, 17. listopadu 2172/15, 708 00 Ostrava-Poruba, Czech Republic
[2]Nanotechnology Centre and IT4Innovations, Technical University Ostrava, 17. listopadu 2172/15, 708 00 Ostrava-Poruba, Czech Republic
*petr.hlubina@vsb.cz

Abstract: We report on a one-dimensional photonic crystal (1DPhC) represented by a multilayer structure used for a surface plasmon-like sensing based on Bloch surface waves and radiation modes employing a structure comprising a glass substrate and four bilayers of TiO_2/SiO_2 with a termination layer of TiO_2. We model the reflectance responses in the Kretschmann configuration with a coupling prism made of BK7 glass and express the reflectances for both (*s* and *p*) polarizations in the spectral domain for various angles of incidence to show that a sharp dip associated with the Bloch surface wave (BSW) excitation is obtained in *p* polarization when an external medium (analyte) is air. For *s*-polarized wave BSW is not excited and a shallow dip associated with the guided mode excitation is obtained for a liquid analyte (water). For decreasing angle of incidence, the dip depth is substantially increased, and resonance thus obtained is comparable in magnitude with resonance commonly exhibited by SPR-based sensors. In addition, we revealed that the resonances in *s*-polarization are obtained for other analytes. The surface plasmon-like sensing concept was verified experimentally in the Kretschmann configuration for the guided mode transformed into the radiation mode with a negative and constant sensitivity of −169 nm/RIU, and a detection limit of 5.9×10^{-5} RIU.

1. Introduction

Bloch surface waves (BSWs) exist at the interface between a truncated periodic multilayer system [1] as a one-dimensional photonic crystal (1DPhC) or Bragg mirror, and a dielectric external medium [2–4]. Light confinement in BSWs, which occurs near the multilayer surface, is caused by total internal reflection (TIR) from homogeneous layer and is related to the bandgap of the photonic crystal. This is in contrast with surface plasmon resonance (SPR) phenomenon [5,6], which is based on the generation of the surface plasmon polaritons (SPPs) and propagation of surface plasmon wave along the interface between a dielectric and a thin metal film, such as gold or silver. The field of SPs decays exponentially on both sides of the boundary so that the SPR phenomenon is attractive to sensing in various fields of interest [7–12]. Recently, a type of surface waves at the interface between a metal and a dielectric Bragg mirror, which is referred to as a Tamm plasmon (TP), has been studied [13]. In contrast to the SPPs, TPs can be optically excited by both *s*- and *p*-polarized waves, and moreover, a direct excitation from free space is possible [14–16].

BSWs offer several possible advantages compared to SPPs [4]. BSW can be excited by both *s*- and *p*-polarized waves [17] at any wavelength by suitably changing the geometry and materials of the photonic crystal. In addition, because BSW-based sensors do not rely on the use of metals, the sensors enable sharper resonances than conventional SPR sensors [6]. Finally,

#373156 https://doi.org/10.1364/OME.9.004009
Journal © 2019 Received 18 Jul 2019; revised 9 Aug 2019; accepted 9 Aug 2019; published 10 Sep 2019

Optical Materials EXPRESS

with an appropriate choice of the dielectric materials of the photonic crystal, sensors based on BSWs are mechanically and chemically robust, offering the possibility of operation in aggressive environments. Consequently, Bloch surface waves have emerged as an alternative to SPPs and have been used with various sensing schemes [18–26], including phase-based sensing [19–22] and intensity-based biosensing [23–26]. Additionally, the accessible surface area of a BSW structure can be increased using a porous dielectric, which results in improved sensitivity toward small molecules [27,28]. More recently, fiber optic sensors with multilayer structures have been reported [29–32], including configurations in which multilayer structures have been deposited on a tapered fiber [29], on the outer surface of optical fiber [30], at the tip of a single-mode fiber [31], and inside of a photonic crystal fiber [32].

In this paper, a one-dimensional photonic crystal (1DPhC) represented by a multilayer structure, which is used for a surface plasmon-like sensing based on BSWs and radiation modes, is analyzed theoretically and experimentally. The reflectance responses of both *s*- and *p*-polarized waves in the Kretschmann configuration with a coupling prism made of BK7 glass are modeled, provided that the structure comprising a glass substrate with four bilayers of TiO_2/SiO_2 and a termination layer of TiO_2 is characterized by a method of spectral ellipsometry. The reflectance of *p*-polarized wave as a function of angle of incidence on the prism base is evaluated, demonstrating the presence of a sharp dip associated with the BSW when an external medium (analyte) is air. For *s*-polarized wave BSW is not excited and we demonstrate for a standard analyte (water) the presence of a shallow dip associated with the guided mode excitation. Moreover, for the decreased angle of incidence, the enhanced electromagnetic field is irradiated from the structure, which is accompanied by resonance comparable in magnitude with the SPR resonance. We also revealed and experimentally confirmed that the resonances are resolvable for analytes such as air and aqueous solutions of ethanol in water. We verified the new sensing concept and measured the reflectance responses of the 1DPhC in the Kretschmann configuration, and revealed for the guided mode transformed into the radiation mode that a sensitivity of −169 nm/RIU and a detection limit of 5.9×10^{-5} RIU, respectively, were achieved.

2. Material characterization

The multilayer structure under study was primarily prepared as interference filter whose reflection spectrum is with a central bandpass approximately 118 nm wide (from 504 to 622 nm). A technique of thin film deposition by sputtering was employed (Meopta, Czech Republic), and in order to model the response of the multilayer structure under study, the physical parameters of all the layers were specified. In the first step, the structure was inspected by a scanning electron microscope (FEI Quanta 650 FEG, USA) and it was revealed as demonstrated in Fig. 1(a) that the structure consists of four bilayers of TiO_2/SiO_2 with different thicknesses and a termination layer of TiO_2.

Next, using a method of spectral ellipsometry, variable angle spectroscopic ellipsometric (VASE) data obtained by ellipsometer RC2 (J. A. Woollam Co., Inc., USA) were processed to determine the thicknesses of the layers provided that the refractive index and extinction coefficient dispersion are known or were also characterized employing software EASE (J. A. Woollam Co., Inc., USA). The determined thicknesses are shown in Fig. 1(b) and agree well with the values estimated using a scanning electron microscope (SEM) photo shown in Fig. 1(a).

Using the ellipsometric data, the dispersion properties of a glass substrate were described by a Cauchy formula

$$n(\lambda) = a + b\lambda^{-2} + c\lambda^{-4}, \tag{1}$$

where λ is the wavelength in μm and the values of coefficients a, b, c obtained by the VASE were: $a = 1.5051$, $b = 4.8034 \times 10^{-3}$ μm^2 and $c = 5.9353 \times 10^{-5}$ μm^4.

Optical Materials EXPRESS

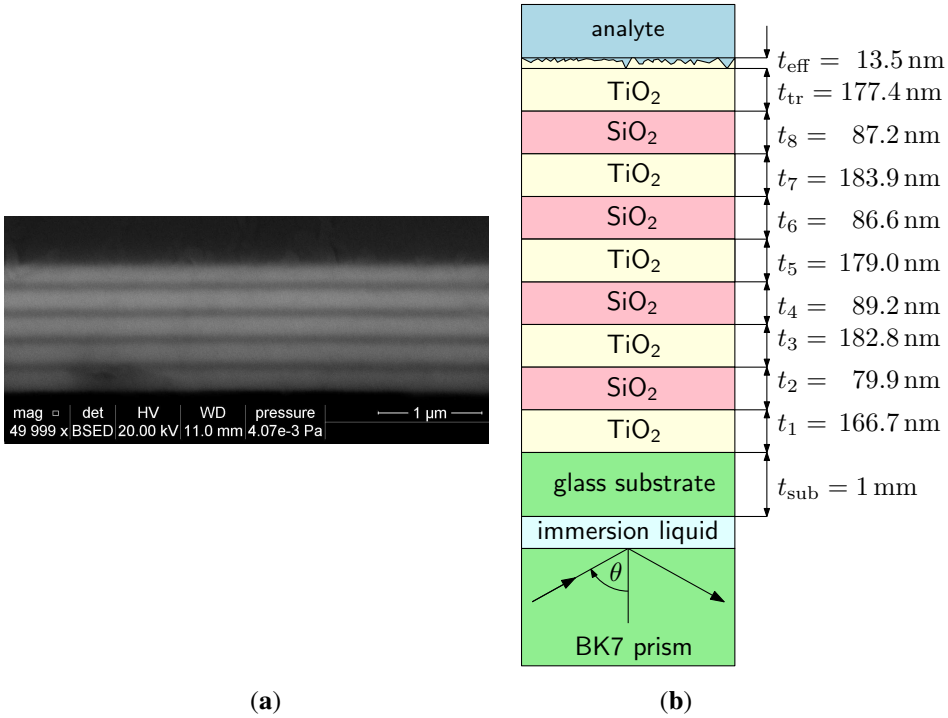

Fig. 1. An SEM photo of a multilayer structure (a), and the geometric representation of the structure (b).

Similarly, for the dispersion properties of TiO_2 and SiO_2 layers, a one-oscillator Sellmeier formula was used

$$n^2(\lambda) = a + \frac{b\lambda^2}{\lambda^2 - c^2}, \tag{2}$$

where λ is the wavelength in μm and a, b, c are the Sellmeier coefficients. Their values for the TiO_2 layers obtained by the VASE were: $a = 2.7655$, $b = 2.2$ and $c = 0.26524$ μm. For SiO_2 we used a model with $a = 1.34836$, $b = 0.75650$ and $c = 0.10683$ μm. The extinction coefficients for TiO_2 and SiO_2 obtained by the VASE were $\kappa_{TiO_2} = \kappa_{SiO_2} \approx 0$. The dispersion of a coupling prism made of BK7 glass was expressed by a three-oscillator Sellmeier formula [33].

3. Theoretical model

To express the optical response of the multilayer structure described in a previous section, a transfer matrix method (TMM) [34] was used. To describe the reflection or transmission properties of the structure, we express the complex reflection/transmission coefficients via the complex amplitudes U of incident (I), reflected (R), transmitted (T) and backward incident (B) waves, which are coupled by a total transmission matrix $\mathbf{M}$ of the structure:

$$\begin{bmatrix} U_{\mathrm{I}}^{(0)} \\ U_{\mathrm{R}}^{(0)} \end{bmatrix} = \begin{bmatrix} M_{11} & M_{12} \\ M_{21} & M_{22} \end{bmatrix} \begin{bmatrix} U_{\mathrm{T}}^{(N+1)} \\ U_{\mathrm{B}}^{(N+1)} \end{bmatrix}, \tag{3}$$

where

$$\mathbf{M} = \mathbf{D}_0^{-1} \left[\prod_{j=1}^{N} \mathbf{D}_j \mathbf{P}_j \mathbf{D}_j^{-1}, \right] \mathbf{D}_{N+1} \tag{4}$$

Optical Materials EXPRESS

and where $\mathbf{D}_j$ are dynamical matrices, $\mathbf{P}_j$ are propagation matrices [34], and indices 0 and $N+1$ refer to the first and last semi-infinite media. In Eq. (4), the dynamical matrices are given by

$$\mathbf{D}_j = \begin{cases} \begin{pmatrix} 1 & 1 \\ k_j & -k_j \end{pmatrix} \text{for } s \text{ wave}, \\ \begin{pmatrix} 1 & 1 \\ \frac{k_j}{n_j^2} & -\frac{k_j}{n_j^2} \end{pmatrix} \text{for } p \text{ wave}, \end{cases} \tag{5}$$

where

$$k_j = \left[\left(n_j \frac{\omega}{c} \right)^2 - \left(n_0 \frac{\omega}{c} \sin\theta \right)^2 \right]^{1/2}. \tag{6}$$

Similarly, the propagation matrices are given by

$$\mathbf{P}_j = \begin{pmatrix} e^{\mathrm{i}k_j t_j} & 0 \\ 0 & e^{-\mathrm{i}k_j t_j} \end{pmatrix}, \tag{7}$$

where t_j is the thickness of j-th layer.

The required complex refection coefficient is expressed using total transmission matrix elements

$$r = \frac{M_{21}}{M_{11}}, \tag{8}$$

and the reflectance R is given by

$$R = |r|^2. \tag{9}$$

4. Theoretical results

To model the spectral responses of the multilayer structure, first we consider air as analyte and angle of incidence θ exceeding the critical angle for the external medium ($\theta_c \approx 41.1°$). Taking into account the dispersion of materials of the structure specified above, and assuming that the extinction coefficients for TiO_2 and SiO_2 layers are $\kappa_{TiO_2} = 1.6 \times 10^{-3}$ and $\kappa_{SiO_2} = 3.4 \times 10^{-4}$ [20], respectively, as an example, Fig. 2 shows the theoretical spectral reflectance of p-polarized wave for angles of incidence θ of light onto the base of the BK7 glass prism ranging from 45° to 49°. As can be seen from Fig. 2(a), sharp dips are obtained and they are shifted toward shorter wavelengths as the angle of incidence increases. Similarly, they are shifted toward longer wavelengths as the angle of incidence is decreasing to θ_c. The dip with the maximum depth, which is located in the center of a short-wavelength bandpass (see the inset of Fig. 2(a) for s-polarized wave and the angle of incidence $\theta = 45°$), is associated with an excitation of the BSW and the remaining dips are due to the response of guided modes in the multilayer system [35]. The shift of the dip can simply be explained for an infinite periodic system [36] when the light line is with increasing slope as the angle of incidence decreases, and thus its intersection with the surface mode line shifts to lower frequency (longer wavelength). The resonance curve parameters such as the depth and the full width at half maximum are determined by the extinction coefficients of layers, and by the coupling efficiency between the launched light and the BSW [20].

To confirm the surface wave resonance at an angle of incidence of 45°, the normalized optical field intensity $|E|^2 / |E_0|^2$ (E_0 is the incident electric field) in the structure at a wavelength of 470.5 nm is shown in Fig. 2(b). This figure clearly demonstrates optical field enhancement in the structure. It is worth noting that the number of the bilayers in our system, which is 4, leads to a slightly different shape of the envelope than is usual when the semi-infinite structure of periodic

Optical Materials EXPRESS

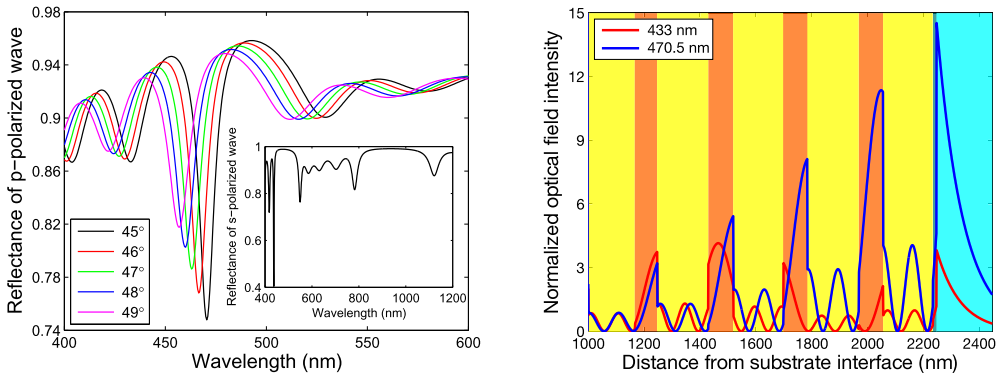

Fig. 2. Theoretical spectral reflectance of p-polarized wave at different angles of incidence θ: 45° to 49° (a). The normalized optical field intensity distribution at angle of incidence $\theta = 45°$ (b). Analyte is air.

bilayers is considered. Similarly, the normalized intensity distribution of guided mode field in the multilayer is demonstrated at a wavelength of 433 nm. The guided mode exhibits more than a four-fold enhancement of the optical intensity with respect to the incident beam, while the BSW shows nearly a fifteen-fold enhancement. These results can also be obtained by a finite element method using commercial software COMSOL Multiphysics [37]. In both cases, an exponential tail in the analyte (air) is obtained with amplitude greater for the surface wave. Consequently, the structure can be used as an optical sensor.

From a point of view of sensing applications, it is required to know spectral responses for analytes with refractive indices near one. Figure 3(a) shows the theoretical spectral reflectance of p-polarized wave for angle of incidence $\theta = 45°$ and analytes with refractive indices ranging from 1 to 1.05. The reflectances have sharp dips with the resonance wavelength shifting toward longer wavelengths as the refractive index increases. Figure 3(b) shows the resonance wavelength as a function of the refractive index and in the same figure is also shown the fitting function (a second-order polynomial). It is evident that the resonance wavelength is with a greater shift for a higher refractive index and the non-linear response in Fig. 3(b) indicates that the sensitivity to the refractive index S_n, defined as the change of the position of the dip $\delta\lambda_r$ with respect to the change of the refractive index δn of the analyte

$$S_n = \frac{\delta\lambda_r}{\delta n}, \tag{10}$$

is linearly refractive index unit (RIU)-dependent. The sensitivity ranges from 100 to 235 nm/RIU and is lower than in the case of the SPR (1050 to 2110 nm/RIU [11]), but is higher compared to TPs (55 nm/RIU [15]). Similar behavior exhibits the detection limit (DL) [10], which is in the best case 4.3×10^{-5} RIU when we consider that the resonance wavelength is resolved with a precision of 0.01 nm.

We extended our analysis to s-polarized wave when analyte is air and revealed that BSW is not excited in a wavelength range from 400 to 1000 nm. In addition, we considered angles of incidence for which the normal component of wavevector of optical wave in the external medium (analyte) is real. In this case, the BSW as a guided mode, with light confined at the multilayer structure surface by TIR from the homogenous medium, cannot be excited. The response is simply a Fabry-Perot-like interference associated with the multilayer structure [38]. As an example, Fig. 4(a) shows the theoretical spectral reflectance for angle of incidence $\theta = 41°$ and analytes with refractive indices ranging from 1 to 1.05. The reflectance dip with the maximum

Optical Materials EXPRESS

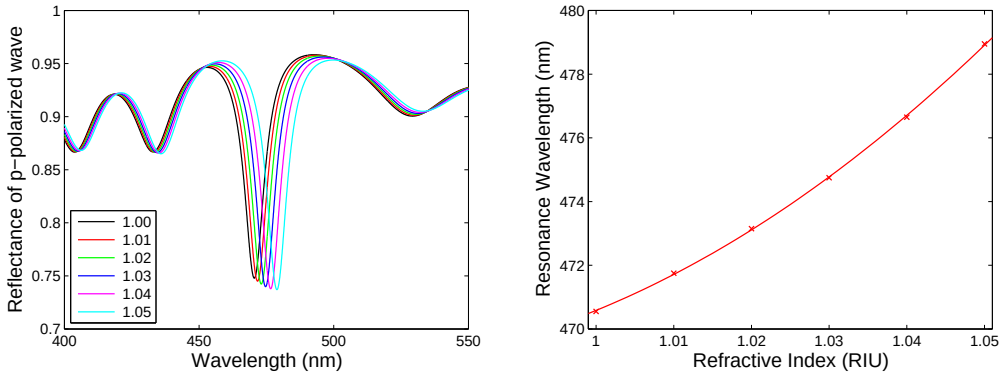

Fig. 3. Theoretical spectral reflectance of p-polarized wave for different refractive indices of analyte when $\theta = 45°$ (a). The resonance wavelength as a function of the refractive index of the analyte with solid line as a fit (b).

depth is located at a short-wavelength edge of a central bandpass and its width increases with the refractive index. The sharp resonance is comparable in magnitude with resonance commonly exhibited by SPR sensors [39]. Contrary to the previous case, the resonance wavelength shifts toward shorter wavelengths as the refractive index increases. The shift can be simply explained by a modification of the guided mode line as the refractive index increases so that its intersection with the light line shifts toward higher frequency (shorter wavelength). Figure 4(b) shows the resonance wavelength as a function of the refractive index together with a linear fitting function. The sensitivity to the refractive index and the detection limit reach -47 nm/RIU and 2.1×10^{-4} RIU, respectively.

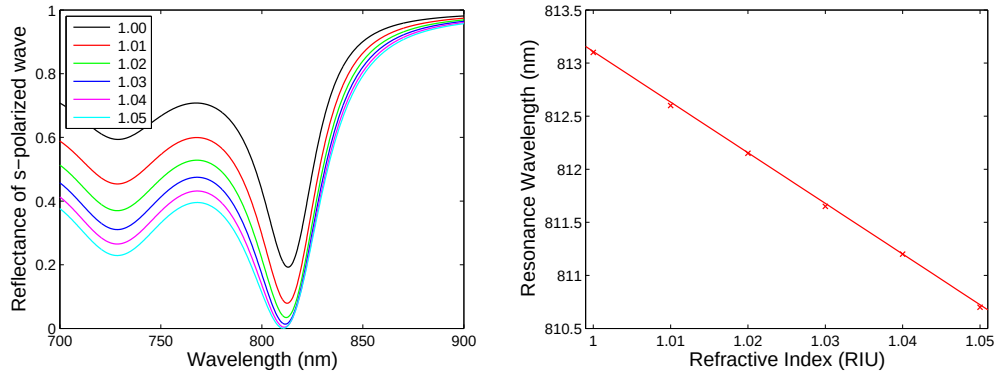

Fig. 4. Theoretical spectral reflectance of s-polarized wave for different refractive indices of analyte when $\theta = 41°$ (a). The resonance wavelength as a function of the refractive index of the analyte with solid line as a fit (b).

Next, to model the spectral responses of the multilayer structure, we consider water as analyte. We revealed that for the structure the BSW is not excited in the considered spectral range (400 to 1000 nm). We focused on the responses of some of the guided modes of the structure. Consequently, Fig. 5(a) shows the theoretical spectral reflectance of s-polarized wave for angles of incidence θ of light onto the base of the BK7 glass prism ranging from 62.5° to 66.5°. As can

Optical Materials EXPRESS

be seen from Fig. 5(a), shallow dips are obtained and they are shifted toward shorter wavelengths as the angle of incidence increases. The shift can be simply explained when the light line is with increasing slope as the angle of incidence decreases, and thus its intersection with the guided mode line shifts to lower frequency (longer wavelength).

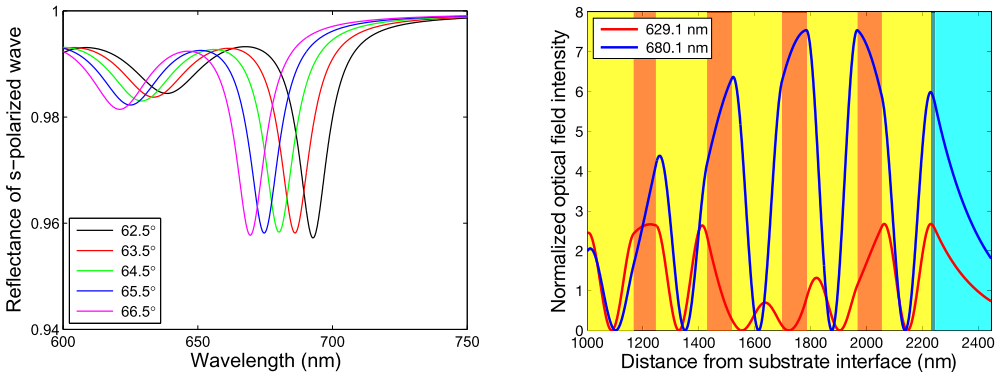

(a) (b)

Fig. 5. Theoretical spectral reflectance of *s*-polarized wave at different angles of incidence θ (a). The normalized optical field intensity distribution at angle of incidence $\theta = 64.5°$ (b). Analyte is water.

To confirm the guided mode resonance at an angle of incidence of 64.5°, the normalized optical field intensity in the structure at a wavelength of 680.1 nm is shown in Fig. 5(b). Similarly, the normalized intensity distribution of guided mode field in the multilayer is illustrated at a wavelength of 629.1 nm. This figure clearly demonstrates optical field enhancement in the structure. The guided modes exhibit more than two- and seven-fold enhancements of the optical intensity with respect to the incident beam.

The spectral responses of the multilayer structure to different analytes are also important. Figure 6(a) shows the theoretical spectral reflectance of *s*-polarized wave for angle of incidence $\theta = 64.5°$ when analytes are the aqueous solutions of ethanol with varying mass concentration of ethanol in water whose dispersion is specified elsewhere [37]. The reflectances have shallow dips with a nearly constant width. The wavelength of the dip (the resonance wavelength) shifts toward longer wavelengths as mass concentration of ethanol in water increases, and the higher the concentration, the smaller is the reflectance at the resonance wavelength. Once again, the shift can be simply explained by change of the guided mode line and its intersection with the light line. Figure 6(b) shows the resonance wavelength as a function of the refractive index of the analyte and in the same figure is also shown the fitting function (a second-order polynomial). It is evident that the resonance wavelength is with a greater shift for a higher refractive index and the non-linear response in Fig. 6(b) indicates that the sensitivity to the refractive index S_n is linearly RIU-dependent and it ranges from 67 to 247 nm/RIU. Similar behavior exhibits the DL, which is in the best case 4×10^{-5} RIU.

It is desirable to extend our analysis to angles of incidence for which a guided mode, even with the enhanced electromagnetic field, is transformed into the radiation mode. Figure 7(a) shows theoretical spectral reflectance of *s*-polarized wave when angle of incidence θ decreases from 61.5° to 57.5°. As can be seen from Fig. 7(a), extrema due to the response of guided modes in the multilayer system and resonance dips are obtained, and they are shifted toward longer wavelengths as the angle of incidence decreases. In addition, the resonances with the maximum depth are due to light irradiation from the structure into the analyte (water) and are affected by optical field enhancement in the structure [40]. In other words, the reflectance decreases to 0

Optical Materials EXPRESS

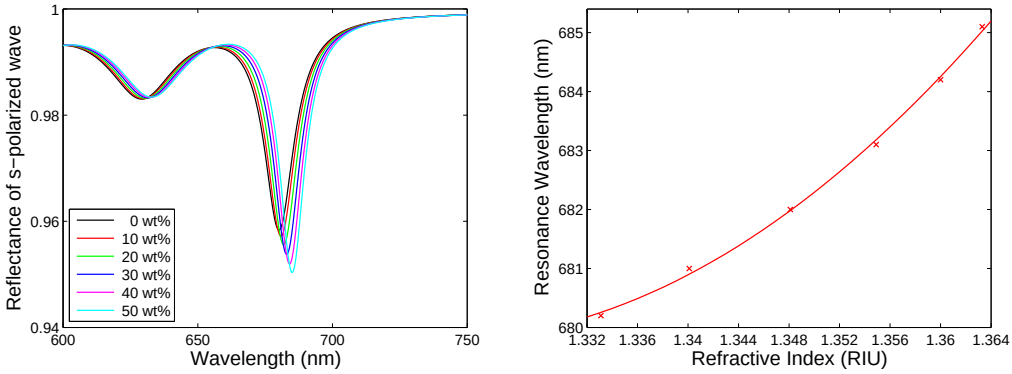

Fig. 6. Theoretical spectral reflectance of *s*-polarized wave for different weight concentrations of ethanol in water when $\theta = 64.5°$ (a). The resonance wavelength as a function of the refractive index of the analyte with solid line as a fit (b).

due to the angle of incidence smaller than the critical angle for the external medium and this is in contrast with the opposite case when the reflectance approaches 1 (see Fig. 5). These dips are comparable in magnitude with resonances commonly exhibited by an SPR [10,11], but are narrower. As an example, a width of 15 nm for $\theta = 61.5°$ is substantially smaller than a width of 65 nm for the SPR responses [11]. The width of the resonances and their depth also change with the angle of incidence. To discriminate between different modes, the normalized optical field intensity distribution at a wavelength of 706.2 nm is shown in Fig. 7(b) for an angle of incidence of 60.5°. It clearly demonstrates optical field enhancement in the structure under study and light irradiation from the structure into the external medium (water). In the same figure, the normalized optical field intensity distribution at a wavelength of 650.3 nm is also shown for another guided mode in the multilayer structure.

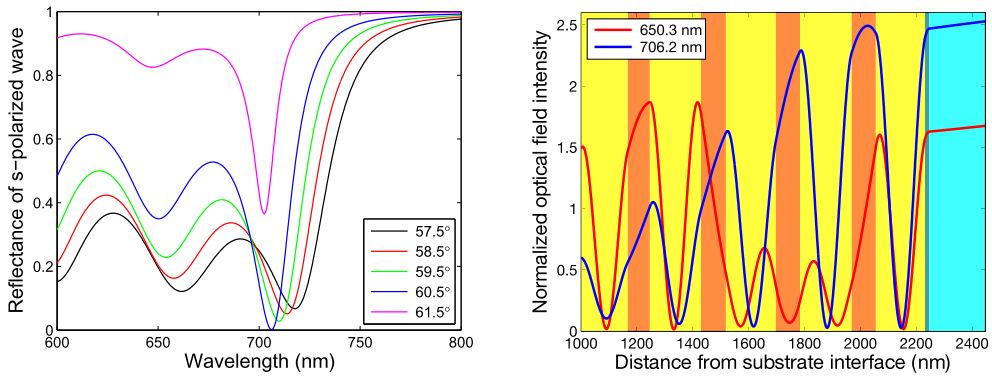

Fig. 7. Theoretical spectral reflectance of *s*-polarized wave at different angles of incidence θ (a). The normalized optical field intensity distribution at angle of incidence $\theta = 60.5°$ (b). Analyte is water.

This case is also important from a point of sensing applications, therefore spectral responses for different analytes are required. Figure 8(a) shows the theoretical spectral reflectance of *s*-polarized wave for angle of incidence $\theta = 61.3°$ and analytes represented by the aqueous solutions of

Optical Materials EXPRESS

ethanol. The reflectances have dips with increasing depth and width as the concentration of ethanol in water in weight percent (wt.%) increases. Contrary to the previous case, the resonance wavelength shifts toward shorter wavelengths as the concentration of ethanol in water increases. Figure 8(b) shows the resonance wavelength as a function of the weight concentration of ethanol and in the same figure is also shown a linear fitting function, which means that the sensitivity to the refractive index given by Eq. (10) is a negative constant and it reaches −108 nm/RIU. This negative sign is opposite to that commonly exhibited by SPR-based sensors. In addition, the DL reaches in this case 9.3 $\times 10^{-5}$ RIU.

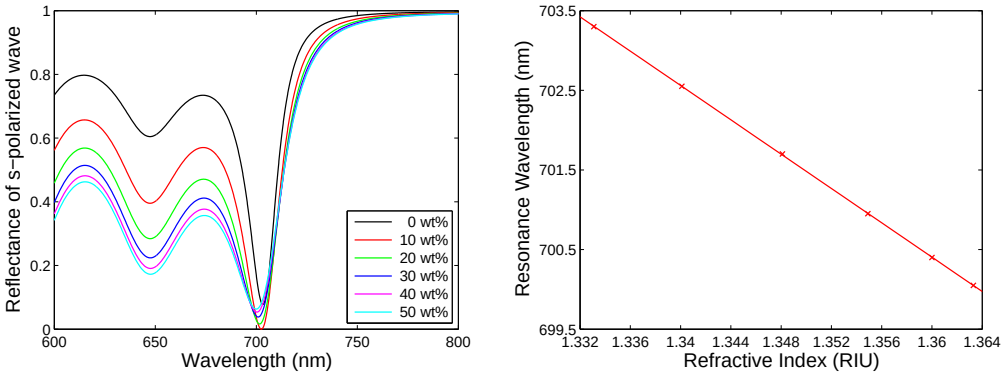

(a) (b)

Fig. 8. Theoretical spectral reflectance of *s*-polarized wave for different weight concentrations of ethanol in water when $\theta = 61.3°$ (a). The resonance wavelength as a function of the refractive index of the analyte with solid line as a fit (b).

5. Experimental setup

An experimental setup used to measure the spectral reflectance of both *s*- and *p*-polarized waves is shown in Fig. 9 and it employs the Kretschmann configuration to resolve the dips associated with an excitation of Bloch surface or radiation waves. White-light source WLS (halogen lamp HL-2000, Ocean Optics, USA) with launching optics, an input optical fiber and collimating lens CL are used to generate a collimated beam of 1 mm diameter which passes through linear polarizer P (LPVIS050, Thorlabs, USA) oriented 45° with respect to the plane of incidence so that both *s*- and *p*-polarized components are present. The light beam is coupled to the multilayer structure under test by equilateral BK7 prism (Ealing, Inc., USA) using a thin layer of index-matching fluid (Cargille, USA, n_D=1.516).

The reflected light passes through linear analyzer A (LPVIS050, Thorlabs, USA) oriented perpendicularly or parallelly to the plane of incidence so that *s*- or *p*-polarized component is detected when the light is launched directly into a read optical fiber (M15L02, Thorlabs, USA) of a spectrometer (USB4000, Ocean Optics, USA). Using the rotary stage, to which the collimator is attached, the angle of incidence can be adjusted [39,41]. If the angle between the incident beam and the normal to the prism face is denoted as α (see Fig. 9), the angle of incidence θ on the base of the equilateral prism is given as

$$\theta = 60° - \sin^{-1}[n_{air}(\lambda_r)\sin\alpha/n(\lambda_r)], \tag{11}$$

where $n_{air}(\lambda_r)$ and $n(\lambda_r)$ and are the refractive indices of air and the prism glass, respectively, at the resonant wavelength λ_r.

As analytes, aqueous solutions of ethanol were prepared. The concentrations of ethanol were 0 (distilled water), 10, 20, 30, 40, and 50 wt.%. The refractive indices of the solutions were

Optical Materials EXPRESS

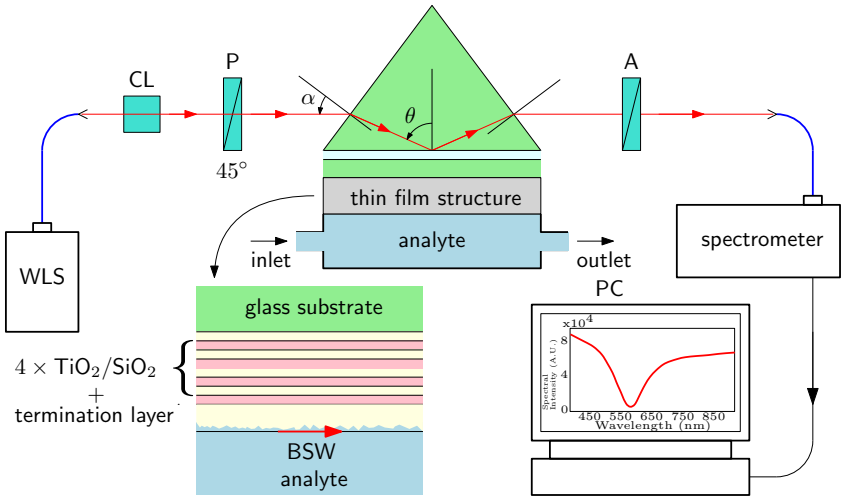

Fig. 9. Experimental setup for measuring the reflectance responses of the multilayer structure in the Kretschmann configuration.

measured at a wavelength of 589.3 nm by refractometer Abbemat MW (Anton Paar GmbH, Austria), and the corresponding refractive indices of 1.33293, 1.33687, 1.33821, 1.34698, 1.35269 and 1.35937 were obtained at a temperature of 22°C.

6. Experimental results and discussion

Utilizing the results of both the material characterization and theoretical modeling, first, angle of incidence α is adjusted to resolve a dip in the reflectance spectrum of *p*-polarized wave for a reference analyte represented by air [39,41]. To diminish the effect of the source spectrum, the recorded spectra were normalized with respect to the spectrum with no effect of both the BSW and guided modes (obtained at a suitable angle of incidence). Examples of the measured reflectance spectra for *p*-polarized component obtained for angles of incidence α ranging from 21.7° to 26.7° are shown in Fig. 10(a). It is clearly seen that a sharp dip due to the BSW excitation is resolved in a wavelength range from 475 to 500 nm. The dip shifts toward shorter wavelengths as the angle of incidence θ increases. Comparing the experimental results with the theoretical ones shown in Fig. 2(a), we confirm good correspondence. Next, Fig. 10(b) shows the measured reflectance spectra of *s*-polarized wave for angles of incidence α ranging from 29° to 34°. For these angles the dip is located at a short-wavelength edge of a central bandpass and is with a greater depth indicating the transformation of the guided mode to the radiation mode and light irradiation from the structure. Also in this case, the dips shift toward shorter wavelengths as the angle of incidence θ increases.

The measurements were extended to analytes represented by aqueous solutions of ethanol in water. Examples of the normalized reflectance spectra for *s*-polarized component obtained for the angle of incidence $\alpha = -5.5°$ ($\theta \approx 63.6°$) are shown in Fig. 11(a). It is clearly seen that a shallow dip due to the guided mode is resolved in a wavelength range from 680 to 720 nm and it shifts toward longer wavelengths as the weight concentration of ethanol diluted in water increases, and the higher the concentration, the deeper is the reflectance spectrum. These results are in agreement with the theoretical ones shown in Fig. 6(a). Figure 11(b) shows the corresponding resonance wavelength as a function of the refractive index of analyte together with a fitting function (a second-order polynomial). It indicates that the resonance wavelength is with a greater shift for a higher refractive index and the sensitivity S_n given by Eq. (10) increases

Optical Materials EXPRESS

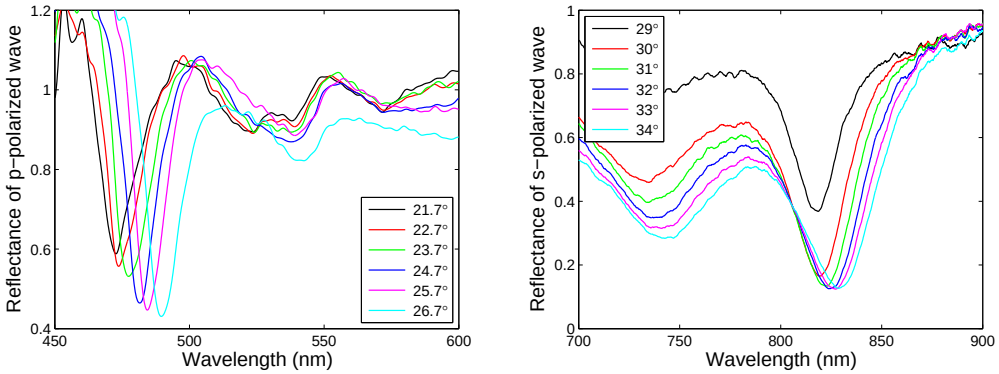

(**a**) (**b**)

Fig. 10. Measured spectral reflectance at different angles of incidence α, p-polarized wave (a), s-polarized wave (b). Analyte is air.

in the considered wavelength range from 100 to 191 nm/RIU. The DL reaches in the best case 5.2×10^{-5} RIU. Comparing the experimental results with the theoretical ones, we confirm good correspondence.

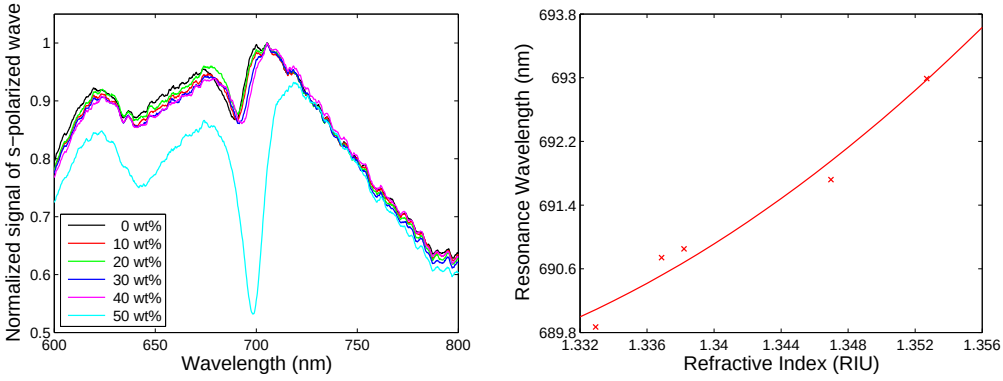

(**a**) (**b**)

Fig. 11. Measured spectral reflectance of s-polarized wave for different weight concentrations of ethanol in water when $\alpha = -5.5°$ (a). The resonance wavelength as a function of the refractive index of the aqueous solution of ethanol with solid line as a fit (b).

In Fig. 11(a) is also shown the response related to analyte represented by 50 wt.% of ethanol in water. The maximum depth is the result of the transformation of the guided mode to the radiation mode (the angle of incidence is smaller than the critical angle for the external medium). Thus, the measurement was extended to angles for which the normal component of the wavevector in analyte is real so that the radiation mode propagates. Examples of the reflectance spectra for s-polarized component obtained for the angle of incidence $\alpha = -2°$ ($\theta \approx 61.3°$) are shown in Fig. 12(a). It is evident that a dip with a sufficiently great depth is resolved in a wavelength range from 680 to 730 nm and it shifts toward shorter wavelengths as the weight concentration of ethanol diluted in water increases, and higher the concentration, the wider is the reflectance dip. Figure 12(b) shows the corresponding resonance wavelength as a function of the refractive index of analyte together with a linear fitting function. The sensitivity and the DL reach −169

Optical Materials EXPRESS

nm/RIU and 5.9×10^{-5} RIU, respectively. Once again, comparing the experimental results with the theoretical ones shown in Figs. 8(b) and 8(b), respectively, we revealed good correspondence.

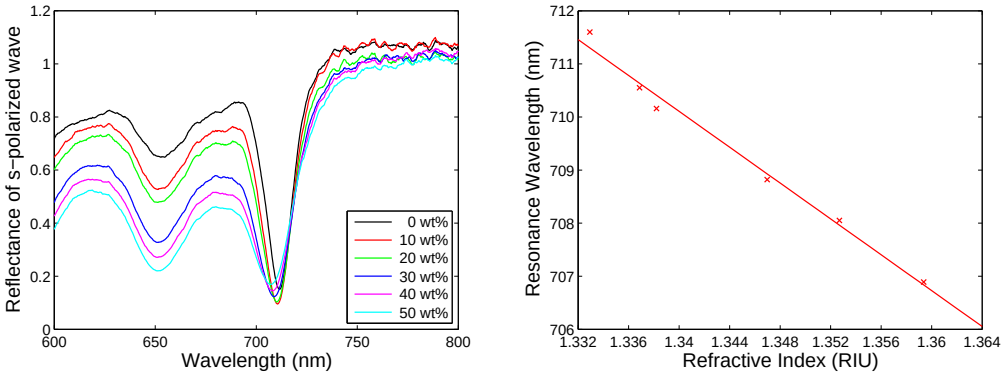

(**a**) (**b**)

Fig. 12. Measured spectral reflectance of *s*-polarized wave for different weight concentrations of ethanol in water when $\alpha = -2^\circ$ (a). The resonance wavelength as a function of the refractive index of the aqueous solution of ethanol with solid line as a fit (b).

7. Conclusions

In this paper, a 1DPhC represented by a multilayer structure and used for a surface plasmon-like sensing based on BSWs and radiation modes has been analyzed theoretically and experimentally. The reflectance responses in the Kretschmann configuration with a coupling prism made of BK7 glass have been modeled using the results obtained from material characterization of the structure by spectral ellipsometry. We demonstrated for *p*-polarized wave and a reference analyte (air) the presence of a sharp dip associated with the BSW excitation. We also demonstrated for *s*-polarized wave conversion of the guided mode to the radiation mode, or equivalently irradiation of the enhanced electromagnetic field from the structure, with resonances comparable in magnitude with the SPR ones. We revealed and experimentally confirmed that the guided and radiation mode resonances are resolvable for other analytes such as aqueous solutions of ethanol in water. The new sensing concept is supported by the measured reflectance responses of the 1DPhC in the Kretschmann configuration, giving a constant sensitivity of −169 nm/RIU and a detection limit of 5.9×10^{-5} RIU, respectively.

The use of the proposed concept, which has advantages in more pronounced reflection dips and a linear response to refractive index changes, can be extended, for example, for measuring the phase response employing a standard phase technique [10,11] or a full ellipsometric approach [20]. In addition, the parameters of a multilayer structure can be optimized to attain better detection limit.

Funding

European Regional Development Fund; European Social Fund.

Acknowledgements

The research was supported by ERDF/ESF project New Composite Materials for Environmental Applications (No. CZ.02.1.01/0.0/0.0/17_048/0007399), and by the student grant system through project SP2019/26. D. V. and P. K. acknowledge the scholarship of the city of Ostrava,

Optical Materials EXPRESS

support from Czech Science Foundation (project 18-22102) and the student grant system (project SP2019/92).

References

1. P. Yeh, A. Yariv, and A. Y. Cho, "Optical surface waves in periodic layered media," Appl. Phys. Lett. **32**(2), 104–105 (1978).
2. R. D. Meade, K. D. Brommer, A. M. Rappe, and J. D. Joannopoulos, "Electromagnetic Bloch waves at the surface of a photonic crystal," Phys. Rev. B **44**(19), 10961–10964 (1991).
3. E. Guillermain, V. Lysenko, R. Orobtchouk, T. Benyattou, S. Roux, A. Pillonnet, and P. Perriat, "Bragg surface wave device based on porous silicon and its application for sensing," Appl. Phys. Lett. **90**(24), 241116 (2007).
4. A. Sinibaldi, N. Danz, E. Descrovi, P. Munzert, U. Schulz, F. Sonntag, L. Dominici, and F. Michelotti, "Direct comparison of the performance of Bloch surface wave and surface plasmon polariton sensors," Sens. Actuators, B **174**, 292–298 (2012).
5. J. Homola, S. Yee, and G. Gauglitz, "Surface plasmon resonance sensors: review," Sens. Actuators, B **54**(1-2), 3–15 (1999).
6. J. Homola, *Surface Plasmon Resonance Based Sensors* (Springer-Verlag, 2006).
7. B. Liedberg, C. Nylander, and I. Lundström, "Principles of biosensing with an extended coupling matrix and surface plasmon resonance," Sens. Actuators, B **11**(1-3), 63–72 (1993).
8. A. Kabashin, S. Patskovsky, and A. Grigorenko, "Phase and amplitude sensitivities in surface plasmon resonance bio and chemical sensing," Opt. Express **17**(23), 21191–212047 (2009).
9. A. Shalabney and I. Abdulhalim, "Figure-of-merit enhancement of surface plasmon resonance sensors in the spectral interrogation," Opt. Lett. **37**(7), 1175–1177 (2012).
10. P. Hlubina, M. Duliakova, M. Kadulova, and D. Ciprian, "Spectral interferometry-based surface plasmon resonance sensor," Opt. Commun. **354**, 240–245 (2015).
11. P. Hlubina and D. Ciprian, "Spectral phase shift of surface plasmon resonance in the Kretschmann configuration: theory and experiment," Plasmonics **12**(4), 1071–1078 (2017).
12. A. A. Rifat, M. Rahmani, L. Xu, and A. E. Miroshnichenko, "Hybrid metasurface based tunable near-perfect absorber and plasmonic sensor," Materials **11**(7), 1091 (2018).
13. M. Kaliteevski, I. Iorsh, S. Brand, R. A. Abram, J. M. Chamberlain, A. V. Kavokin, and I. A. Shelykh, "Tamm plasmon-polaritons: Possible electromagnetic states at the interface of a metal and a dielectric Bragg mirror," Phys. Rev. B **76**(16), 165415 (2007).
14. X.-L. Zhang, J.-F. Song, X.-B. Li, J. Feng, and H.-B. Sun, "Optical Tamm states enhanced broad-band absorption of organic solar cells," Appl. Phys. Lett. **101**(24), 243901 (2012).
15. B. Auguié, M. C. Fuertes, P. C. Angelomié, N. L. Abdala, G. J. A. A. S. Illia, and A. Fainstein, "Tamm plasmon resonance in mesoporous multilayers: Toward a sensing application," ACS Photonics **1**(9), 775–780 (2014).
16. C. Zhang, K. Wu, V. Giannini, and X. Li, "Planar hot-electron photodetection with Tamm plasmons," ACS Nano **11**(2), 1719–1727 (2017).
17. J. Chen, D. Zhang, P. Wang, H. Ming, and J. R. Lakowicz, "Strong polarization transformation of Bloch surface waves," Phys. Rev. Appl. **9**(2), 024008 (2018).
18. M. Liscidini and J. E. Sipe, "Analysis of Bloch-surface-wave assisted diffraction-based biosensors," J. Opt. Soc. Am. B **26**(2), 279–289 (2009).
19. Y. Li, T. Yang, S. Song, Z. Pang, and G. Du, "Phase properties of Bloch surface waves and their sensing applications," Appl. Phys. Lett. **103**(4), 041116 (2013).
20. A. Sinibaldi, R. Rizzo, G. Figliozzi, E. Descrovi, N Danz, P. Munzert, A. Anopchenko, and F. Michelotti, "A full ellipsometric approach to optical sensing with Bloch surface waves on photonic crystals," Opt. Express **21**(20), 23331–23344 (2013).
21. Y. Li, T. Yang, Z. Pang, G. Du, and S. Song, "Phase-sensitive Bloch surface wave sensor based on variable angle spectroscopic ellipsometry," Opt. Express **22**(18), 21403–21410 (2014).
22. Y. Wan, Z. Zheng, M. Cheng, W. Kong, and K. Liu, "Polarimetric-phase-enhanced intensity interrogation scheme for surface wave optical sensors with low optical loss," Sensors **18**(10), 3262 (2018).
23. A. Farmer, A. C. Friedli, S. M. Wright, and W. M. Robertson, "Biosensing using surface electromagnetic waves in photonic band gap multilayers," Sens. Actuators, B **173**, 79–84 (2012).
24. W. Kong, Z. Zheng, Y. Wan, S. L. a, and J. Liu, "High-sensitivity sensing based on intensity-interrogated Bloch surface wave sensors," Sens. Actuators, B **193**, 467–471 (2014).
25. X. B. Kanga, L. Wen, and Z. G. Wang, "Design of guided Bloch surface wave resonance bio-sensors with high sensitivity," Opt. Commun. **383**, 531–536 (2017).
26. T. Kovalevich, D. Belharet, L. Robert, G. Ulliac, M.-S. Kim, H. P. Herzig, T. Grosjean, and M.-P. Bernal, "Bloch surface waves at the telecommunicationwavelength with Lithium Niobate as top layer forintegrated optics," Appl. Opt. **58**(7), 1757–1762 (2019).
27. H. Qiao, B. Guan, J. J. Gooding, and P. J. Reece, "Protease detection using a porous silicon based Bloch surface wave optical biosensor," Opt. Express **18**(14), 15174–15182 (2010).

Optical Materials EXPRESS

28. G. A. Rodriguez, J. D. Ryckman, Y. Jiao, and S. M. Weiss, "A size selective porous silicon grating-coupled Bloch surface and sub-surfacewave biosensor," Biosens. Bioelectron. **53**, 486–493 (2014).
29. T. Tu, F. Panf, S. Zhu, J. Cheng, H. Liu, J. Wen, and T. Wang, "Excitation of Bloch surface wave on tapered fiber coated with one-dimensional photonic crystal for refractive index sensing," Opt. Express **25**(8), 9019–9027 (2017).
30. X.-J. Tan and X.-S. Zhu, "Optical fiber sensor based on Bloch surface wave in photonic crystals," Opt. Express **24**(14), 16016–16026 (2016).
31. M. Scaravilli, A. Micco, G. Castaldi, G. Coppola, M. Gioffre, M. Iodice, V. L. Ferrara, V. Galdi, and A. Cusano, "Excitation of Bloch surface waves on an optical fiber tip," Adv. Opt. Mater. **6**, 1800477 (2018).
32. E. Gonzalez-Valencia, R. A. Herrera, and P. Torres, "Bloch surface wave resonance in photonic crystal fibers: towards ultra-wide range refractive index sensors," Opt. Express **27**(6), 8236–8545 (2019).
33. http://refractiveindex.info.
34. P. Yeh, *Optical Waves in Layered Media* (J. Wiley and Sons, Inc., 1988).
35. M. Shinn and W. Robertson, "Surface plasmon-like sensor based on surface electromagnetic waves in a photonic band-gap material," Sens. Actuators, B **105**(2), 360–364 (2005).
36. F. Villa, L. E. Regalado, F. Ramos-Mendieta, J. Gaspar-Armenta, and T. Lopez-Ríos, "Photonic crystal sensor based on surface waves for thin-film characterization," Opt. Lett. **27**(8), 646–648 (2002).
37. M. Gryga, D. Ciprian, and P. Hlubina, "Surface electromagnetic wave sensor utilizing a one-dimensional photonic crystal," Proc. SPIE **11028**, 110281P (2019).
38. K. V. Popov, J. A. Dobrowolski, A. V. Tikhonravov, and B. T. Sullivan, "Broadband high-reflection multilayer coatings at oblique angles of incidence," Appl. Opt. **36**(10), 2139–2151 (1997).
39. R. Chlebus, J. Chylek, D. Ciprian, and P. Hlubina, "Surface plasmon resonance based measurement of the dielectric function of a thin metal film," Sensors **18**(11), 3693 (2018).
40. D. Aurelio and M. Liscidini, "Electromagnetic field enhancement in Bloch surface waves," Phys. Rev. B **96**(4), 045308 (2017).
41. P. Hlubina, M. Lunackova, and D. Ciprian, "Phase sensitive measurement of the wavelength dependence of the complex permittivity of a thin gold film using surface plasmon resonance," Opt. Mater. Express **9**(3), 992–1001 (2019).